

Discovery of Novel *N*-Phenylphenoxyacetamide Derivatives as EthR Inhibitors and Ethionamide Boosters by Combining High-Throughput Screening and Synthesis

Marion Flipo,^{†,‡,§,||,⊥,⊞} Nicolas Willand,^{†,‡,§,||,⊥,⊞} Nathalie Lecat-Guillet,^{†,||,⊥,⊞,∇,○}
Candide Hounsou,^{†,‡,§,||,⊥} Matthieu Desroses,^{†,‡,§,||,⊥} Florence Leroux,^{†,‡,§,||,⊥} Zoé Lens,^{†,◆,¶}
Vincent Villeret,^{†,◆} Alexandre Wohlkönig,[□] René Wintjens,[●] Thierry Christophe,^{▲,☆}
Hee Kyoung Jeon,[▲] Camille Lochet,^{†,||,⊥,∇,○} Priscille Brodin,^{†,||,⊥,∇,○,▲} Alain R Baulard,^{†,||,⊥,⊞,∇,○,⊞}
and Benoit Déprez^{*,†,‡,§,||,⊥,⊞}

[†]Université Lille Nord de France, F-59000 Lille, France

[‡]Biostructures and Drug Discovery, Institut National de la Santé et de la Recherche Médicale (INSERM) U761, F-59000 Lille, France

[§]Université Droit & Santé (UDSL), F-59000 Lille, France

^{||}Institut Pasteur de Lille, F-59019 Lille, France

[⊥]Pôle de Recherche Interdisciplinaire sur le Médicament (PRIM), F-59000 Lille, France

[#]INSERM U1019, F-59000 Lille, France

[∇]Centre National de Recherche Scientifique (CNRS) UMR8204, F-59021 Lille, France

[○]Center for Infection and Immunity of Lille, F-59019 Lille, France

[◆]Institut de Recherche Interdisciplinaire (IRI), CNRS USR3078, F-59658 Villeneuve d'Ascq, France

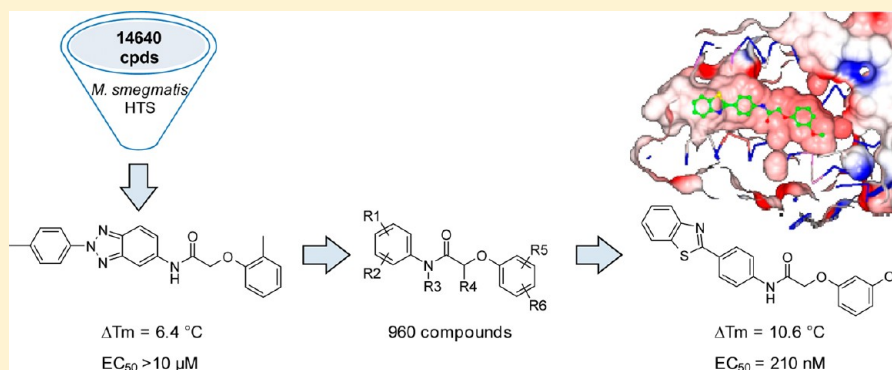
[¶]Laboratory of Molecular Virology, Institut de Biologie et de Médecine Moléculaires (IBMM), Université Libre de Bruxelles (ULB), 6041 Gosselies, Belgium

[▲]Biology of Intracellular Pathogens INSERM-Avenir, Institut Pasteur Korea (IPK), 463-400 Gyeonggi-do, South Korea

[□]Structural Biology Brussels and Molecular and Cellular Interactions, Vlaams Instituut voor Biotechnologie (VIB), 1050 Brussels, Belgium

[●]Laboratoire des Biopolymères et des Nanomatériaux Supramoléculaires, Institut de Pharmacie, ULB, 1050 Brussel, Belgium

S Supporting Information



ABSTRACT: In this paper, we describe the screening of a 14640-compound library using a novel whole mycobacteria phenotypic assay to discover inhibitors of EthR, a transcriptional repressor implicated in the innate resistance of *Mycobacterium tuberculosis* to the second-line antituberculosis drug ethionamide. From this screening a new chemical family of EthR inhibitors bearing an *N*-phenylphenoxyacetamide motif was identified. The X-ray structure of the most potent compound crystallized with EthR inspired the synthesis of a 960-member focused library. These compounds were tested in vitro using a rapid thermal shift assay on EthR to accelerate the optimization. The best compounds were synthesized on a larger scale and confirmed as potent ethionamide boosters on *M. tuberculosis*-infected macrophages. Finally, the cocrystallization of the best optimized analogue with EthR revealed an unexpected reorientation of the ligand in the binding pocket.

Received: March 19, 2012

Published: June 28, 2012

■ INTRODUCTION

Tuberculosis (TB) remains a major cause of mortality, killing 1.7 million people each year.¹ In 2010, TB incidence and prevalence were estimated by the World Health Organization (WHO) at 8.8 and 12 million cases, respectively.¹ Difficulties in detecting and curing enough cases to interrupt transmission are the biggest obstacles in controlling this infection.² One-third of the world population is infected with the latent form of *Mycobacterium tuberculosis*, and approximately 10% will develop the disease.³ The directly observed treatment short course (DOTS), a multidrug therapy program developed by the WHO, covers approximately 77% of the world's population and contributes to controlling the epidemic.^{4,5} Nevertheless, the treatment success rate remains below the target of 90%,¹ particularly in Africa.⁶ Moreover, the global HIV infection epidemic has contributed to the explosive increase of TB incidence and the emergence of multi-drug-resistant (MDR) strains. In 2010, the number of MDR-TB infections was estimated at 650 000 cases.¹ MDR-TB patients must be treated for 2–4 years with several second-line drugs, which are less effective and poorly tolerated, weakening observance and leading to treatment failure. In the past 40 years no new antituberculosis drugs have succeeded in reaching the market, and there is an urgent need for new molecules, particularly ones that shorten the treatment time and cure patients with multi-drug-resistant and extensively drug resistant strains.⁷

■ BOOSTING ETHIONAMIDE APPROACH

Current TB therapies include a large number of prodrugs that must be metabolically transformed by the mycobacteria to manifest their activity. One of these, ethionamide, an antibiotic used to treat multi-drug-resistant TB, is bioactivated by the mycobacterial monooxygenase EthA.^{8,9} The active bacterial metabolite of ethionamide^{10–12} inhibits InhA,^{13,14} the enoyl-acyl carrier protein (ACP) reductase involved in mycolic acid biosynthesis. The limited effectiveness of ethionamide has been explained by the transcriptional repression of *ethA* exerted by the bacterial regulator EthR.¹⁵ Thus, EthR contributes to the innate resistance of *M. tuberculosis* to this antibiotic. EthR was proposed and validated as a drug target to boost the bioactivation of ethionamide and potentiate the drug in vivo.¹⁶ We recently reported structure–activity relationships of a series of druglike 1,2,4-oxadiazole EthR inhibitors identified through a rational drug design approach.^{17,18} This led to the discovery of highly potent boosters both in vitro on the targeted protein EthR and ex vivo on the human pathogen *M. tuberculosis* in a macrophage-infected model. Another study performed in parallel revealed that the ligand-binding pocket of EthR can accommodate

compounds twice as long as the previous 1,2,4-oxadiazoles by reorganizing residues hiding an unexplored cavity.¹⁹ These compounds opened new frontiers for the development of high-affinity EthR inhibitors. Knowing that target-based approaches do not account for permeability, we wanted to use a high-throughput assay that would have the potential to reveal new chemotypes with a good capacity to cross the complex mycobacterial envelope. Here, we report the screening of a library of 14 640 compounds using a whole mycobacterial phenotypic assay that led to the discovery of an *N*-phenylphenoxyacetamide family. The optimization of this series was driven by the synthesis of a 960-member focused library that was screened on EthR using a rapid thermal shift assay.

■ ASSAY DESIGN AND SCREENING

We previously demonstrated that the inhibition of EthR by synthetic ligands correlates with its incapacity to bind to the DNA operator controlling the expression of the monooxygenase coding gene *ethA*.¹⁶ To exploit this as a read-out assay for the identification of EthR inhibitors in mycobacteria, we used the nonpathogenic fast-growing TB surrogate *Mycobacterium smegmatis*. The *ethA* promoter/operator was inserted into a mycobacterial shuttle vector upstream of the glucuronidase reporter gene (*uidA*). Introduced in *M. smegmatis*, this vector led to the expression of *uidA*, which was easily detected using the profluorescent substrate 4-methylumbelliferyl β -D-glucuronide (MUG). In contrast, when this clone was transformed with a second plasmid overexpressing *ethR* of *M. tuberculosis*, a total disappearance of the glucuronidase activity was observed. A 14640-compound library purchased from Asinex and ChemDiv was screened using this assay at 10 μ M to identify potent EthR inhibitors through their capacity to trigger the expression of *uidA* (Figure 1).

At the end of the screening process, 76 compounds were identified as potent reactivators of the glucuronidase activity in *M. smegmatis* through inhibition of EthR. These 76 hits and 244 chemical analogues picked out of the 14640-compound library were selected for dose–response experiments to recover potential false-negative compounds. Among the 320 compounds, 22 showed IC₅₀ values below 10 μ M and were tested using a thermal shift assay on purified EthR (Figure 2).

This fluorescence-based assay was developed to confirm that hit compounds actually bind to the target protein EthR.²⁰ The principle of the thermal shift assay lies in the monitoring of the thermal unfolding of the protein using a conformation-sensitive dye, SYPRO Orange, in which fluorescence is quenched in aqueous solution but enhanced in a nonpolar environment, such as the hydrophobic domain of a protein that begins to unfold. The assay is carried out on standard Q-PCR instruments in

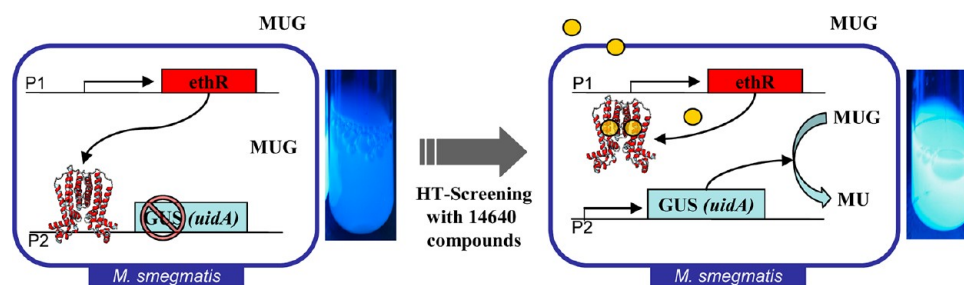


Figure 1. Fluorescent assay used for the screening of the library. *M. smegmatis* is transformed with plasmid P1 overexpressing *ethR* and with plasmid P2 expressing *uidA* under the control of the promoter/operator of *ethA*. In the absence of EthR inhibitors, EthR binds to the promoter/operator, which blocks the transcription of *uidA*. MUG is not hydrolyzed. Compounds of the library (shown as yellow balls) that penetrate into the bacteria and inhibit EthR release the production of UidA, which cleaves MUG in fluorescent methylumbelliferone (MU) and glucuronic acid.

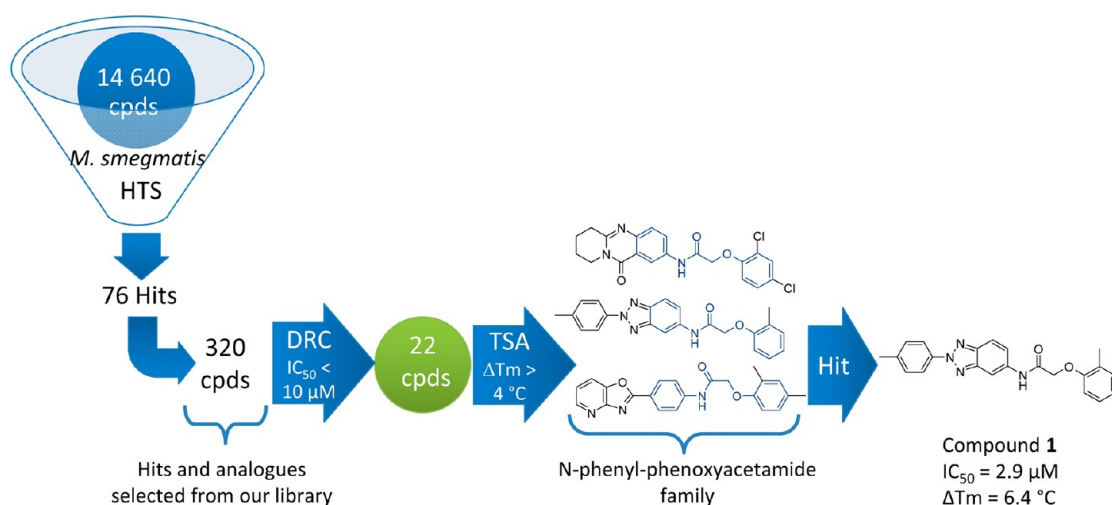


Figure 2. Screening cascade developed for the identification of compound **1** as an EthR inhibitor.

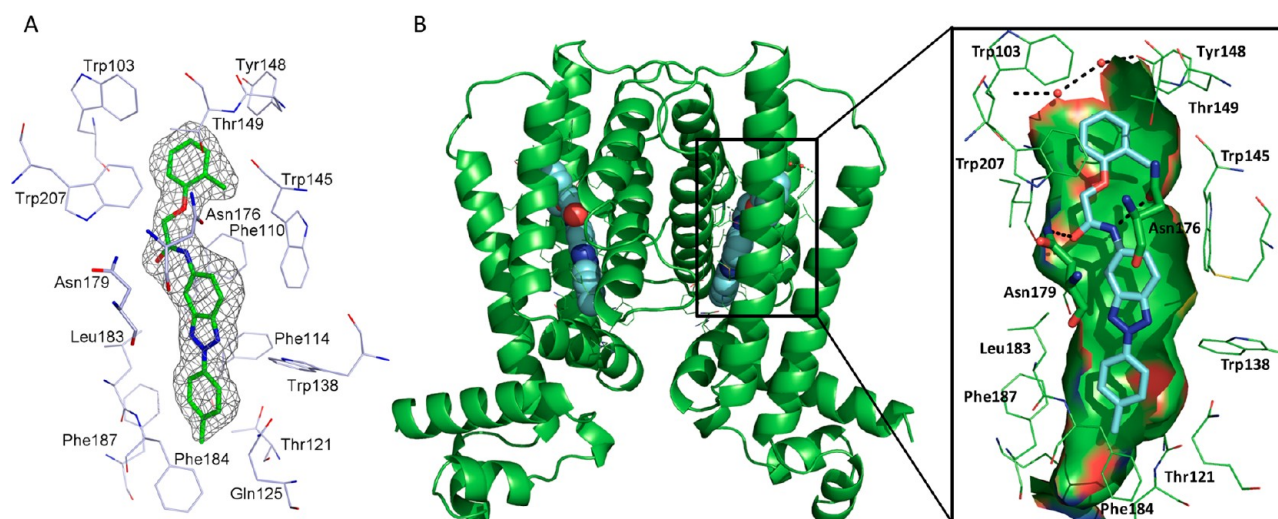


Figure 3. (A) X-ray structure representation of the ligand-binding pocket of EthR filled with compound **1** (PDB ID 3Q3S) surrounded by its initial $F_o - F_c$ map at the 3.0σ contour level. The $F_o - F_c$ map was calculated prior to addition of the ligand to the model. (B) X-ray structure representation of the homodimeric conformation of EthR filled in both monomers with compound **1**. The surface of the ligand binding domain is highlighted. Hydrogen bonds with Asn179 and Asn176 are represented with dotted lines. Color legend: blue (compound **1**) or green (EthR) = carbon, dark blue = nitrogen, red = oxygen, yellow = sulfur. The images were generated with Pymol.

96-well plates. Results are produced as graphs showing the fluorescence intensity of SYPRO Orange as a function of the temperature. The inflection of the sigmoid curve indicates the melting temperature (T_m) of the protein. The variation of the melting temperatures between holoprotein and apoprotein (ΔT_m) reflects the capacity of the ligand to stabilize the receptor protein in a liganded conformation.^{21–25} From the 22 compounds identified through the glucuronidase *M. smegmatis* assay, six produced a significant ΔT_m (greater than 4°C). Among them three were members of the *N*-phenylphenoxyacetamide family (Figure 2). Compound **1** (Figure 2) showed the best activities in the two assays ($IC_{50} = 2.9 \mu\text{M}$ and $\Delta T_m = 6.4^\circ\text{C}$).

Compound **1** was cocrystallized with the protein. X-ray diffraction revealed that the *N*-phenylphenoxyacetamide motif is the key pharmacophore for binding. Indeed, the amide function of the ligand is hydrogen bonded to the side chains of the two asparagines, Asn179 and Asn176 (Figure 3). The *o*-methylphenoxy moiety of the ligand occupies the upper hydrophobic pocket formed by the side chains of Trp207, Thr149, Leu187, and Gly106, a

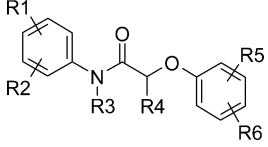
region involved in the induction of the structural reorganization of the helix–turn–helix (HTH) motifs of EthR.²⁰ The benzotriazole motif faces Phe110 and Phe114, while the third remaining aromatic ring in contact with Trp138 and Phe187 invades a small hydrophobic pocket thanks to the rotation of Phe184. The existence of this cavity, not explored by compounds in our first series, was previously shown by the cocrystal structure of EthR with hexadecyl octanoate²⁶ and by the study of EthR flexibility using in situ click chemistry experiments.¹⁹ As expected, the crystal structure revealed the repressor in a conformation incompatible with DNA binding. Indeed, the distance between the two HTH motifs (50.5 \AA) is consistent with the phenotypic screening result.

To rapidly optimize the pharmacodynamic properties of this new chemical family of EthR inhibitors, we designed a focused library based on the *N*-phenylphenoxyacetamide motif. The amide bond and the ether bond of the structure are two obvious disconnection points amenable to high-throughput synthesis. Diversity was thus introduced via a large set of commercially available anilines and phenols.

LIBRARY DESIGN AND SYNTHESIS

Anilines bearing various substituents were selected to generate diverse pharmacophoric patterns. Secondary amines, cyclic or acyclic, were also incorporated into the library, as well as amines displaying two aromatic rings or anilines with acidic and basic functions. Phenols with electron-withdrawing or electron-donating groups on the ring were selected. Bulkier phenols displaying naphthyl or adamantyl groups were also chosen to fill the 3D diversity space. The 960-member virtual library was enumerated using Pipeline Pilot. Druglike properties such as the polar surface area (PSA), the number of rotatable bonds, clogP, the molar mass, and the number of hydrogen bond donors and acceptors were calculated for each member (Table 1). All the

Table 1. Calculated Properties of the Library Members^a



	mean	std dev	range
molar mass (g/mol)	340.6	48.7	227.3–497.6
clogP	3.7	1.1	0.9–6.9
no. of H-bond acceptors	3.2	1.0	2–6
no. of H-bond donors	1.0	0.5	0–3
no. of rotatable bonds	5.5	1.3	3–10
PSA (Å ²)	56.2	18.1	29.5–118.4

^aAll the properties were calculated using Pipeline Pilot from Accelrys.

library members were compliant with Veber's rules and Lipinski's rule-of-five.^{27–29}

The chemical synthesis of the library was developed according to an optimized two-step synthesis protocol. The first step consisted of an acetylation of anilines with chloroacetyl chloride or 2-chloropropionyl chloride following a known procedure³⁰ using dimethylacetamide as the solvent (Scheme 1A) to yield (2-chlorophenyl)acetamide and (2-chlorophenyl)propionamide (Table 2).

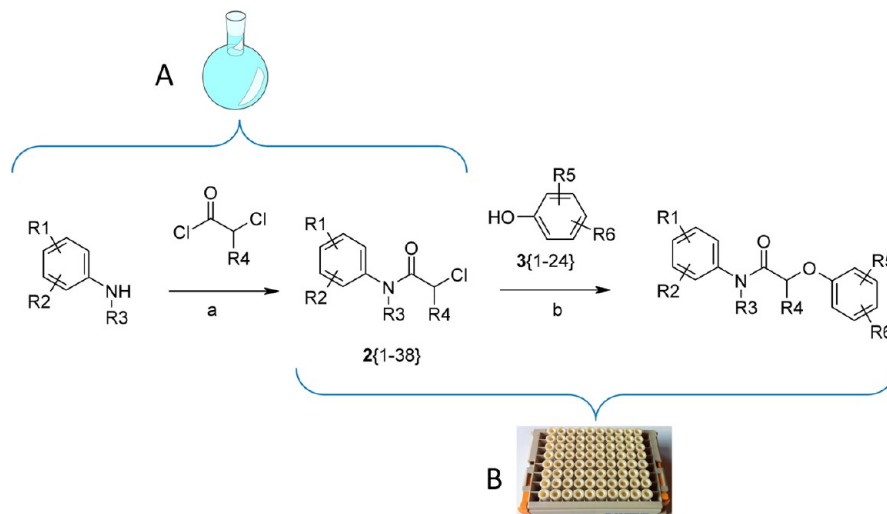
In the second step, phenols 3[1–24] (Table 3) were alkylated by 2-chloro-*N*-phenylacetamides 2[1–32] and 2-chloro-*N*-phenylpropionamides 2[33–38] to yield the final compounds. The conditions for the alkylation were first investigated by studying the reaction of 2-chloro-*N*-phenylacetamide 2[1] with phenol 3[1]. A variety of reaction conditions were explored to improve the conversion and avoid the alkylation of the amide function. The chloroacetamide 2[1] was sufficiently reactive, and the use of a catalyst such as KI, NaI, KBr, or NaBr did not improve the reaction. K₂CO₃ was established as the most efficient base for this reaction. The use of Cs₂CO₃ increased the formation of the *N*-alkylated byproduct. On the contrary, the use of DIEA or KOH led to complex mixtures. Polar aprotic solvents such as CH₃CN and DMF were established as the best solvents for this reaction. DMF was preferred due to the higher solubility of the starting materials and therefore its application in automated parallel synthesis, especially to dispense solution. It was found that heating was required to obtain a total conversion. Finally, phenols 3[1–24] were deprotonated using potassium carbonate in DMF (0.5 M) at room temperature, and the alkylation with chloroacetamides 2[1–32] and chloropropionamides 2[33–38] performed at 50 °C for 96 h led to the synthesis of the 960-compound library (Scheme 1B). Chloroacetamides 2[19] and 2[20] were incorporated twice in the library to obtain both protected and free carboxylic and amino derivatives thanks to the cleavage of *tert*-butyl and Boc groups in acidic conditions (50% TFA in CH₂Cl₂).

The synthesis of the library was carried out in 2D barcoded tubes (Matrix) on a scale of 20 μmol, and the solutions of the reactants in DMF were distributed using an automated liquid-handling system (Tecan Genesis RSP 150). A total of 118 wells were randomly analyzed by LC–MS to show that for 96% of the analyzed library members the purity was higher than 80% (see the Supporting Information).

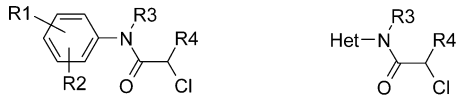
SCREENING RESULTS OF THE *N*-PHENYLPHENOXYACETAMIDE LIBRARY

The library was screened using the thermal shift assay described previously. Out of the 960 compounds screened at 20 μM,

Scheme 1. (A) Synthesis of 2-Chloroacetamide and 2-Chloropropionamide 2[1–38]^a and (B) Automated Parallel Synthesis of the *N*-Phenylphenoxyacetamide Library (960 Members)^a



^aReaction conditions: (a) DMA, 0 °C, then rt, 1–5 h; (b) phenol (0.5 M)/DMF (1 equiv), K₂CO₃ (2 equiv), 1 h, rt, then chloroacetamide (0.5 M)/DMF (1 equiv), 96 h, 50 °C.

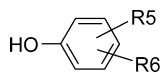
Table 2. Structures of (2-Chlorophenyl)acetamides 2[1–32] and (2-Chlorophenyl)propionamides 2[33–38]


compd	R1	R2	R3	R4
2[1]	H	H	H	H
2[2]	4-Me	H	H	H
2[3]	2-OMe	H	H	H
2[4]	3-OMe	H	H	H
2[5]	4-OMe	H	H	H
2[6]	4-Cl	H	H	H
2[7]	3-Cl	4-Cl	H	H
2[8]	3-CF ₃	H	H	H
2[9]	4-CF ₃	H	H	H
2[10]	3-CN	H	H	H
2[11]	4-CN	H	H	H
2[12]	4-Ph	H	H	H
2[13]	4-OPh	H	H	H
2[14]	2-OPh	4-OEt	H	H
2[15]	3-CONHPh	H	H	H
2[16]	3,4-(–OCH ₂ O–)	H	H	H
2[17]	4-morpholin-4-yl	H	H	H
2[18]	4-(2-oxopyrrolidin-1-yl)	H	H	H
2[19]	4-CH ₂ NH-Boc	H	H	H
2[19] ^a	4-CH ₂ NH ₂	H	H	H
2[20]	4-CH ₂ COOtBu	H	H	H
2[20] ^a	4-CH ₂ COOH	H	H	H
2[21]	2-Ph	H	H	H
2[22]	4-benzothiazol-2-yl	H	H	H
2[23]	3-pyrimidin-5-yl	H	H	H
2[24]	Het = 9-ethyl-9H-carbazol-3-yl	H	H	H
2[25]	Het = 2-methylquinolin-6-yl	H	H	H
2[26]	Het = 1-methyl-1H-indol-5-yl	H	H	H
2[27]	Het = 2-(trifluoromethyl)-1H-benzimidazol-5-yl	H	H	H
2[28]	H	H	CH ₃	H
2[29]	4-OMe	H	CH ₃	H
2[30]	H	H	CH ₂ Ph	H
2[31]	H	H	cyclohexyl	H
2[32]	H	2-(CH ₂ CH ₂ CH ₂ –)	H	H
2[33]	H	H	H	CH ₃
2[34]	4-Me	H	H	CH ₃
2[35]	4-OMe	H	H	CH ₃
2[36]	4-Cl	H	H	CH ₃
2[37]	3-Cl	4-Cl	H	CH ₃
2[38]	4-Ph	H	H	CH ₃

^aChloroacetamides 2[19'] and 2[20'] were added to the table to symbolize free carboxylic and free amino analogues of chloroacetamides 2[19] and 2[20].

38 were found to induce a positive shift in the melting temperature of the complex higher than the one observed with reference compound 1. The distribution of shifts observed for the entire library is presented in Table 4.

Figure 4 displays ranges of ΔT_m according to the chloroacetamide and phenol building block series. Small temperature shifts were obtained with chloropropionamides methylated on the α -position (2[33–38]) compared to the nonmethylated series (Figure 4A). Free carboxylic acid and amino groups (2[19'], 2[20']) were not well tolerated compared to their protected analogues (2[19], 2[20]). Substitution of the amide function on the nitrogen atom by a bulky group such as benzyl

Table 3. Structures of Phenols 3[1–24]


compd	R5	R6	compd	R5	R6
3[1]	H	H	3[13]	4-CN	H
3[2]	2-Me	H	3[14]	2-OMe	H
3[3]	4-Me	H	3[15]	3-OMe	H
3[4]	2-F	H	3[16]	4-OMe	H
3[5]	3-F	4-F	3[17]	3-NMe ₂	H
3[6]	2-Cl	H	3[18]	3-NHCOPh	H
3[7]	3-Cl	H	3[19]	3-OPh	H
3[8]	4-Cl	H	3[20]	4-Ph	H
3[9]	3-Cl	4-Cl	3[21]	4-adamantyl	H
3[10]	2-CF ₃	H	3[22]	4-(1,2,4-triazol-1-yl)	H
3[11]	4-CF ₃	H	3[23]	2-(1,3,4-oxadiazol-2-yl)	H
3[12]	3-CN	H	3[24]	2,3-C ₄ H ₄	H

Table 4. ΔT_m Distribution of EthR in Complex with the 960 Compounds of the Library

ΔT_m (°C)	no. of compds	fraction of the library (%)	ΔT_m (°C)	no. of compds	fraction of the library (%)
<1	421	43.9	5–7	102	10.6
1–3	248	25.8	7–9	21	2.2
3–5	166	17.3	9–11	2	0.2

or cyclohexyl was deleterious to activity (2[30], 2[31]), and substitution by a methyl group was more tolerated, but nonalkylated analogues led to larger thermal shifts (2[1] vs 2[28] and 2[5] vs 2[29]). Interestingly, cyclization of aniline into 1,2,3,4-tetrahydroquinoline was also tolerated (2[1] vs 2[32]). Substitution on the ortho position of the phenyl was deleterious to activity (2[3], 2[14], 2[21]). Heteroaromatic rings such as 4-benzothiazol-2-ylphenyl (2[22]) and 2-methylquinoline (2[25]) showed good activity as well as 4-phenoxy (2[13]) and 3,4-methylenedioxy (2[16]) groups. Substitution of phenols with 2-chloro-*N*-(3,4-dichlorophenyl)acetamide 2[7] led to the maximum number of compounds that induced a positive shift in the T_m of the protein higher than that of reference compound 1.

Smaller shifts of the melting temperature were obtained with phenols (Figure 4B) bearing heteroaromatic substituents (3[22], 3[23]), a benzamide moiety (3[18]) or a tertiary nitrogen atom (3[17]). The EthR ligand binding domain is a narrow hydrophobic tunnel, so bulky groups such as 1-naphthol (3[24]) or trifluoro and methoxy groups in the ortho position of the phenol (3[10] and 3[14]) were not tolerated as opposed to smaller substituents such as a methyl group and fluorine and chlorine atoms (3[2], 3[4], 3[6]). Para and meta substitutions were well tolerated. 4-(Trifluoromethyl)phenol (3[11]), 3-methoxyphenol (3[15]), and 3-phenoxyphenol (3[19]) derivatives showed a maximum response.

The 23 compounds (2.4% of the library) displaying a shift of the melting temperature higher than 7 °C (Table 4) were selected for resynthesis on a larger scale (0.5 mmol) according to Scheme 1 and retested to confirm the ΔT_m values (Table 5). In parallel, the ability of these 23 compounds (at 10 μ M) to boost a subactive dose of ethionamide (MIC/10) was determined by measuring the replication of *M. tuberculosis* H37Rv-GFP inside macrophages in an automated confocal microscopy assay.^{31–33} The results are expressed as bacterial growth inhibition (%) (Table 5).

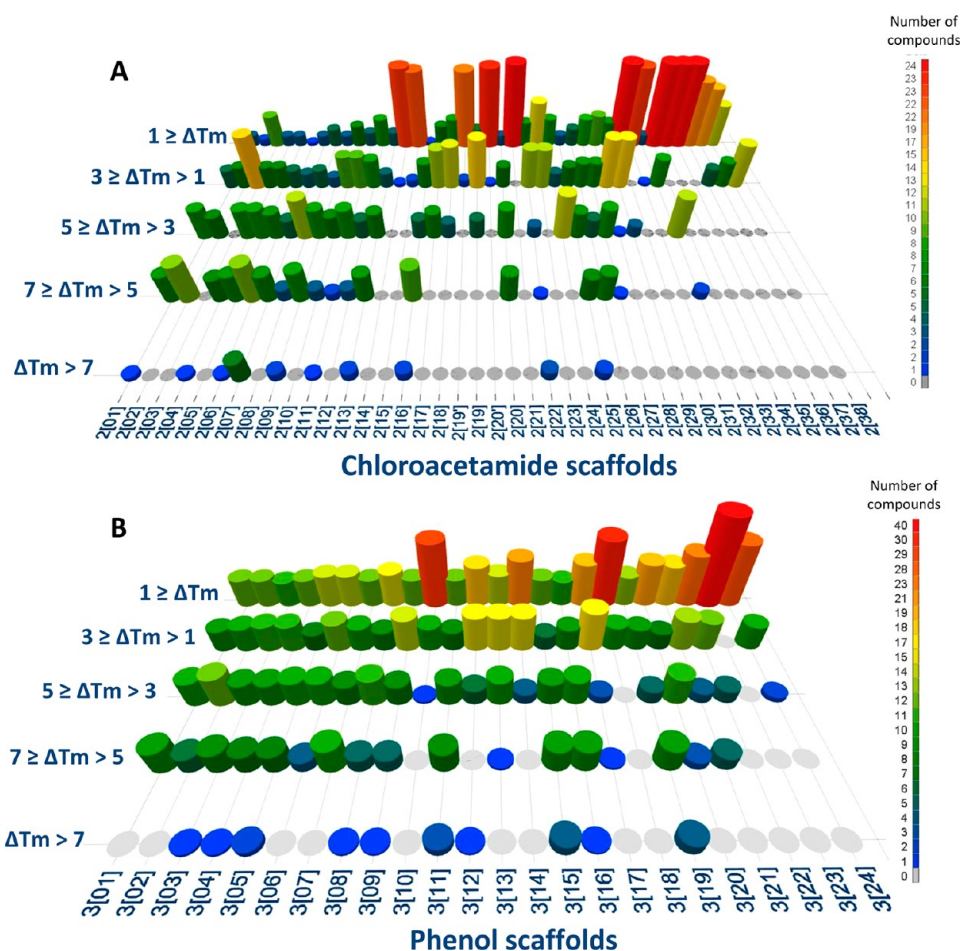


Figure 4. ΔT_m distribution of EthR in complex with the 960-compound library according to (A) chloroacetamide building blocks 2[1–38] or (B) phenol building blocks 3[1–24]. The images were generated with Miner3D.

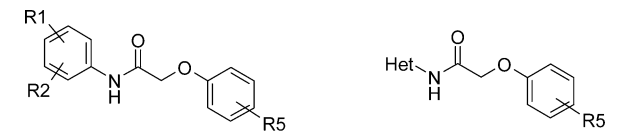
Eight compounds (4, 5, 6, 9, 12, 14, 19, and 22) were reconfirmed as positive as they still displayed ΔT_m greater than 7 °C (Table 5). Among them, two compounds (4 and 5) were active in vitro as potent ethionamide boosters (inh > 50%). Compound 4 was the most active, with $\Delta T_m = 10.6$ °C and inh = 67.6%. Replacement of the lipophilic methoxy group by a more polar cyano group on the phenol ring (compound 5) was less tolerated ($\Delta T_m = 8.1$ °C and inh = 53%). In contrast, in the *N*-(2-methylquinolin-6-yl)acetamide and *N*-(4-chlorophenyl)acetamide series, compounds 15 (inh = 83.2%) and 21 (inh = 92.6%) were active in vitro in the presence of ethionamide with lower ΔT_m values (5.1 and 6.1 °C, respectively). The most active compounds (4, 5, 15, and 21) with inh > 50% at 10 μM were selected for dose–response experiments performed in the presence of ethionamide at 0.1 $\mu\text{g}/\text{mL}$ (MIC/10) on *M. tuberculosis*-infected macrophages (Table 6).³¹

All four compounds were able to boost ethionamide activity 10-fold in TB-infected macrophages with EC_{50} in the micromolar (compounds 15 and 21) or submicromolar (compounds 4 and 5) range. The *N*-(4-benzothiazol-2-ylphenyl)acetamide series presented the best boosters. Compound 4 displaying an EC_{50} of 0.21 μM was at least 50-fold more active than reference compound 1 on TB-infected macrophages in combination with a subactive dose of ethionamide. This compound did not show any antituberculous activity when tested alone at 10 μM (see the Supporting Information, Table 2

on p S8). The role of the phenoxy group was confirmed by the synthesis of the sulfur analogue (compound 27) (Table 6). Compound 27 was obtained according to Scheme 1 using chloroacetamide 2[22] and 3-methoxythiophenol. This compound displayed a ΔT_m lower than that of compound 4 (6.2 °C) and a weak activity ex vivo on TB-infected macrophages ($\text{EC}_{50} > 10$ μM).

Compound 4 was cocrystallized with EthR (Figure 5). X-ray diffraction data revealed that, like compound 1, the amide function of compound 4 is hydrogen bonded to the side chains of Asn179 and Asn176. However, compound 4 has rotated by 180° around the carbonyl function, pointing its *m*-methoxyphenoxy moiety to the bottom of the ligand binding domain. While compound 1 penetrates deeper into the binding pocket with its *p*-toluyl group, filling a small hydrophobic cavity opened by the rotation of Phe184, in the X-ray structure of EthR in complex with compound 4, this Phe184 moves to close the gate and faces the *m*-methoxyphenoxy ring, which also interacts with Trp138 and Phe114. On the other hand, at the portal of the pocket, the phenylbenzothiazole core of compound 4 binds to the side chains of aliphatic Met102 and Val152 and aromatic Trp103 and Tyr148 and occupies a space that was filled in the compound 1–EthR complex with a water network. These additional hydrophobic contacts significantly increase the ligand–protein binding surface and thereby could explain the higher activity of compound 4 relative to compound 1.

Table 5. Biological Activities of Compounds 4–26



compd	R1	R2	R5	ΔT_m^a (°C)	ΔT_m^b (°C)	inh (%) at 10 μM^c
1	Het = 2-(4-methylphenyl)- 2H-1,2,3-benzotriazol-5-yl	2-Me		6.4	6.4	10.9 ± 1.1
4	4-benzothiazol-2-yl	H	3-OMe	9.9	10.6	67.6 ± 0.4
5	4-benzothiazol-2-yl	H	3-CN	8.2	8.1	53.4 ± 7.6
6	3-Cl	4-Cl	3-OPh	8.9	9.1	-1.6 ± 3.7
7	3-Cl	4-Cl	3-OMe	7.0	6.8	26.7 ± 2.2
8	3-Cl	4-Cl	4-OMe	8.1	6.1	-0.6 ± 0.2
9	3-Cl	4-Cl	4-CF ₃	9.6	8.1	-8.4 ± 1.7
10	3-Cl	4-Cl	4-Cl	7.7	6.9	-17.9 ± 20.9
11	3-Cl	4-Cl	4-Me	7.7	6.8	-10.4 ± 5.7
12	3,4-(–OCH ₂ O–)		4-Ph	7.0	7.0	-3.0 ± 0.05
13	3,4-(–OCH ₂ O–)		4-CF ₃	7.5	6.2	1.4 ± 3.2
14	3,4-(–OCH ₂ O–)		3-OPh	8.8	8.2	5.7 ± 4.3
15	Het = 2-methylquinolin-6-yl	2-F		7.2	5.1	83.2 ± 0.9
16	Het = 2-methylquinolin-6-yl	3-OMe		7.2	6.6	6.5 ± 2.4
17	4-OPh	H	3,4-diF	7.3	5.7	-13.5 ± 1.0
18	4-OPh	H	3-OMe	7.6	6.7	-17.5 ± 16.3
19	4-CF ₃	H	3,4-diCl	7.7	7.5	-5.4 ± 2.8
20	4-CF ₃	H	3,4-diF	8.0	5.6	-12.5 ± 6.9
21	4-Cl	H	3-OMe	8.1	6.1	92.6 ± 0.3
22	4-Ph	H	3-OMe	7.0	7.4	-2.9 ± 2.7
23	H	H	3-OPh	7.0	6.1	2.2 ± 4.6
24	4-CN	H	3-OPh	7.0	6.7	-8.9 ± 9.1
25	3-CN	H	3-OPh	7.3	5.7	-7.2 ± 5.8
26	3-OMe	H	4-CF ₃	7.2	5.0	-1.5 ± 0.4

^a ΔT_m from the screening. ^b ΔT_m measured after resynthesis. ^cInh (%) represents the inhibition of *M. tuberculosis* growth in macrophages with a combination of ethionamide at 0.1 $\mu g/mL$ (normal MIC/10) and each ligand at 10 μM . Inh values are the mean of two experiments.

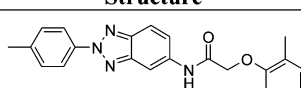
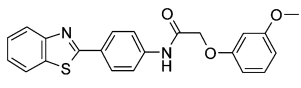
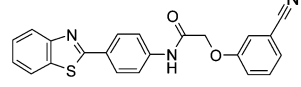
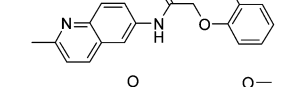
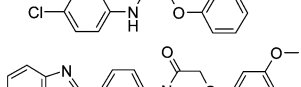
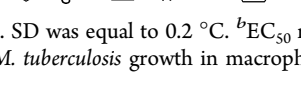
CONCLUSION

In this study, we discovered new EthR inhibitors by the screening of a 14640-compound library on *M. smegmatis*. Compound 1 was shown to be a genuine EthR ligand by X-ray diffraction of a cocrystal. Optimization was made possible by the two-step synthesis of a focused library of *N*-phenylphenoxyacetamide derivatives. The screening of the library on the purified target protein using a thermal shift assay followed by in vitro testing in human macrophages infected by *M. tuberculosis* led to the identification of two potent *N*-(4-benzothiazol-2-ylphenyl)-2-phenoxyacetamide derivatives. Compounds 4 and 5 were at least 50-fold more active than hit compound 1 in boosting a subactive dose of ethionamide on TB-infected macrophages. Finally, the cocrystallization of compound 4 with EthR revealed a new binding mode compared to that of the hit analogue 1. We believe that the development of a screening cascade involving a whole cell phenotypic assay and a target-based physical assay was critical to the discovery and rapid design of new potent EthR inhibitors and could therefore be a valuable tool for the identification of other inhibitors of mycobacterial transcriptional regulators.

EXPERIMENTAL SECTION

Biology. High-Throughput in Bacterio Assay. The shuttle plasmid pMV261 was used to overexpress in *M. smegmatis* the reporter gene *uidA*, which codes for the β -glucuronidase (GUS) of *Escherichia coli*. The promoter/operator sequence of *ethA* was polymerase chain reaction (PCR)-amplified using oligonucleotides O-315 (5' GCC-TCT-AGA-CAG-CGA-AGC-CTG-ACT-GG 3') and O-316 (5' CTC-GGC-CAT-GGA-TCC-ACG-CTA-TCA-AC 3'), which contain restriction sites *Xba*I and *Nco*I, respectively. The PCR product was digested and cloned in plasmid pModTin,³⁴ previously digested with the restriction enzymes *Sca*I and *Nco*I. The resulting plasmid pModTin-PrethA was digested with *Xba*I and *Eco*RV and cloned in pMV261 previously digested with the same enzymes. These manipulations resulted in the mycobacterial shuttle plasmid pMV261-PrethA-Tin (called P2 in Figure 1), in which *uidA* is under the control of the *ethA* promoter/operator.

Table 6. Biological Activities of Compounds 1, 4, 5, 15, 21, and 27

compd	Structure	ΔT_m (°C) ^a	EC ₅₀ (μM) ^b
1		6.4	>10
4		10.6	0.21
5		8.1	0.34
15		5.1	2.2
21		6.1	1.6
27		6.2	>10

^a ΔT_m values are the mean of two experiments. SD was equal to 0.2 °C. ^bEC₅₀ represents the concentration of ligand that allows ethionamide at 0.1 $\mu g/mL$ (normal MIC/10) to inhibit 50% of *M. tuberculosis* growth in macrophages. EC₅₀ values are the mean of two experiments. SD was <10%.

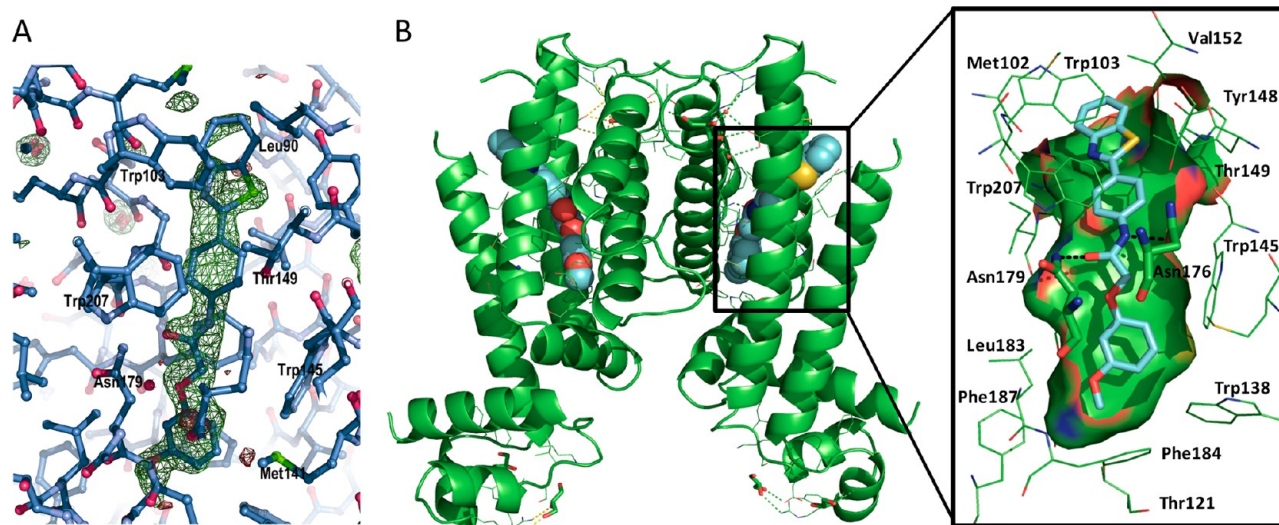


Figure 5. (A) X-ray structure representation of the ligand-binding pocket of EthR filled with compound 4 (PDB ID 4DW6) surrounded by its initial omit $F_o - F_c$ map at the 3.0σ contour level. The $F_o - F_c$ map was calculated prior to addition of the ligand to the model. (B) X-ray structure representation of the homodimeric conformation of EthR filled with compound 4. The surface of the ligand binding domain is highlighted. Hydrogen bonds with Asn179 and Asn176 are represented with dotted lines. Color legend: blue (compound 4) or green (EthR) = carbon, dark blue = nitrogen, red = oxygen, yellow = sulfur. The images were generated with Pymol.

In parallel, plasmid pMV261-ethR described previously⁸ was digested with enzymes *Xba*I and *Spe*I, and the fragment containing *ethR* under the control of the *hsp60* promoter was inserted into the same restriction sites of the single copy number plasmid pBSh-D³⁵ to create pBSh-ethRb (called P1 in Figure 1).

M. smegmatis mc²155³⁶ was transformed with plasmid P2 (pMV261-PrethA-Tin) alone, which resulted in the high production of glucuronidase and was used as a positive control in our screening assay. Alternatively, *M. smegmatis* mc²155 was transformed conjointly with plasmid P2 (pMV261-PrethA-Tin) and plasmid P1 (pBSh-ethRb), in which the production of EthR represses completely the expression of the reporter cassette PrethA-Tin, resulting in the absence of detectable glucuronidase activity. *M. smegmatis* clones were cultivated in Sauton medium supplemented with Triton WR1339.

The high-throughput screen was performed in 96-well plates (Optiplate 96F, Perkin-Elmer) containing in each well 123 μ L of the mycobacterial culture (optical density of 0.2 at 600 nm), 10 μ L of a 50 μ M solution of MUG (Calbiochem), and 67 μ L of a 33 μ M 10% DMSO solution of each compound of the library. The spectrophotometric measure was done after 0, 24, and 48 h of incubation at 37 $^{\circ}$ C using a VICTOR³-V (1420 multilabel counter, Perkin-Elmer) set to an excitation wavelength of 390 nm and an emission wavelength at 405 nm.

Thermal Shift Assay. The fluorescent dye SYPRO Orange (Invitrogen) was used to monitor protein unfolding. This dye is environmentally sensitive and leads to an increase in fluorescence following exposure of hydrophobic regions during protein unfolding. The thermal shift assay was conducted in a Lightcycler 480 (Roche). The system contained a heating/cooling device for temperature control and a charge-coupled device (CCD) detector for real-time imaging of the fluorescence changes in the wells of the microplate. The final sample concentrations were 10 μ M EthR, 2.5 \times SYPRO Orange, 1% DMSO, and 20 μ M ligand in the EthR buffer. The samples were heated from 37 to 85 $^{\circ}$ C with a heating rate of 0.04 $^{\circ}$ C/s. The fluorescence intensity was measured at Ex/Em = 465/510 nm. The data were obtained using the algorithmic program Wavemetrics Igor by applying the following designed procedure: The fluorescence intensity of each well/sample is plotted as a function of the temperature. Then the 1D numerical derivative of these curves is calculated. At last, the maximum data values, corresponding to the inflection points (T_m), are extracted to give T_m in a table and in a graph.

Intracellular Assay. Raw264.7 macrophages (10^8 cells) were infected with an H37Rv-GFP suspension at a multiplicity of infection (MOI) of 1:1 in 300 mL for 2 h at 37 $^{\circ}$ C with shaking (100 rpm). After two washes

by centrifugation at 1100 rpm for 5 min, the remaining extracellular bacilli from the infected cell suspension were killed by a 1 h amikacin (20 μ M, Sigma, A2324-5G) treatment. After a final centrifugation step, 40 μ L of *M. tuberculosis* H37Rv-GFP colonized macrophages were dispensed with the Wellmate (Matrix) into 384-well Evotec plates preplated with 10 μ L of compound mixture diluted in cell medium and incubated for 5 days at 37 $^{\circ}$ C, 5% CO₂. Macrophages were then stained with SYTO 60 (Invitrogen, S11342) for 1 h followed by plate sealing. Confocal images were recorded on an automated fluorescent ultra-high-throughput microscope, Opera (Evotec). This microscope is based on an inverted microscope architecture that allows imaging of cells cultivated in 96- or 384-well microplates (Evotec). Images were acquired with a 20 \times water immersion objective (NA = 0.70). A double laser excitation (488 and 635 nm) and dedicated dichroic mirrors were used to record green fluorescence of mycobacteria and red fluorescence of the macrophages on two different cameras, respectively. A series of four pictures at the center of each well were taken, and each image was then processed using dedicated image analysis.^{31,32} The percentage of infected cells and the number of cells are the two parameters extracted from image analysis as previously reported.³² Reported data are the average of two replicates.

Potency Assay of Test Compounds on *M. tuberculosis* (Ethionamide Concentration Fixed at 0.1 μ g/mL, Serial Dilution of Test Compounds). Ethionamide (Sigma, E6005-5G) was diluted in DMSO at 10 mg/mL, and aliquots were stored frozen at -20 $^{\circ}$ C. Test compounds were resuspended in pure DMSO at a concentration of 4 mg/mL. Ten 2-fold serial dilutions of compounds were subsequently performed in DMSO in Greiner 384-well V-shaped polypropylene plates (Greiner, no. 781280). Equal volumes (5 μ L) of diluted compounds and of ethionamide were transferred to a 384-well low-volume polypropylene plate (Corning, no. 3672). Two independent replicates were done for each setting. On the day of the experiment, 0.5 μ L of compound per plate was transferred by the EVOBird platform (Evotec) to cell assay plates preplated with 10 μ L of assay medium.

Crystal Structure Determination of EthR–Ligand Complexes.

N-terminally hexahistidine-tagged EthR was produced in *E. coli* C41 (pET-15b-ethR) and purified as described. Prior to crystallization, the protein was buffer exchanged against 10 mM Tris-HCl (pH 7.5) and 200 mM NaCl and concentrated to 9 mg/mL. A crystal was obtained by the vapor diffusion method, 0.1 mM MES, pH 6.5, 1.4–1.65 M ammonium sulfate (using a 0.05 M increment), and 10–15% glycerol as the crystallization solution. Ligands were dissolved in 100% DMSO. The EthR–ligand complexes were prepared by mixing 1 μ L of ligand (33 mM) and 9 μ L of protein solution (9 mg/mL) and equilibrated for

Table 7. Data Collection Statistics

	compd 1	compd 4
X-ray source	ESRF ID14-2	SLS
temp (K)	100	100
wavelength (Å)	0.93300	1.00000
space group	P4 ₁ ,2,2	P4 ₁ ,2,2
cell constants (Å)	<i>a</i> = <i>b</i> = 121.2, <i>c</i> = 33.8	<i>a</i> = <i>b</i> = 121.4, <i>c</i> = 33.8
resolution (Å) ^a	2.0 (2.0–2.1)	2.0 (2.0–2.1)
completeness (%)	99.8 (100.0)	99.7 (98.3)
R _{sym} (%)	6.3 (23.0)	5.9 (41.7)
multiplicity	14.1(14.4)	8.8 (9.2)
I/σ(I)	22.6 (5.4)	27.5 (5.6)
no. of total reflns	249020 (33903)	156698 (23020)
no. of unique reflns	17607 (2348)	17743 (2498)

^aThe number in parentheses is the statistic for the highest resolution shell.

30 min at room temperature. All crystals belong to space group P4₁,2,2. Data collection statistics are summarized in Table 7. The diffraction data were processed with XDS. The structure has been refined using REFMAC5³⁷ from the CCP4 suite to the resolution indicated in Table 7. The ligands were positioned in the electron density with Coot.³⁸ The final R_{work} (R_{free}) for compounds 1 and 4 are 18.9% (23.1%) and 18.6% (21.9%), respectively. The analysis of protein–ligand interactions was performed with the aid of the LIGPLOT program.³⁹ PDB access codes are 3Q3S and 4DW6 for compounds 1 and 4, respectively.

Chemistry. General Information. NMR spectra were recorded on a Bruker DRX-300 spectrometer. Chemical shifts are in parts per million (ppm). The assignments were made using 1D ¹H and ¹³C spectra and 2D HSQC and COSY spectra. Mass spectra were recorded with an LC–MSMS triple-quadrupole system (Varian 1200ws) or an LC–MS (Waters Alliance Micromass ZQ 2000). LC–MS analysis was performed using a C18 TSK-GEL Super ODS 2 μm particle size column, dimensions 50 × 4.6 mm, and a 1 mL/min flow rate. The solvent systems used were 100% water containing 0.1% formic acid (solvent A) and a mixture of 20% water and 80% acetonitrile containing 0.1% formic acid (solvent B). A gradient from 100% solvent A to 100% solvent B over 7.5 min was used. The final solvent system was held constant for 1 min. High-resolution mass spectra were recorded on an HPLC–MS-TOF system (Waters LCT Premier). Preparative HPLC was performed using a Varian ProStar system using an OmniSphere 10 column (C₁₈, 250 × 41.4 mm, Dynamax) from Varian, Inc. and a 80 mL/min flow rate. The solvent systems used were 100% water containing 0.1% formic acid (solvent A) and 100% acetonitrile or methanol containing 0.1% formic acid (solvent B). A gradient from 80% solvent A and 20% solvent B to 100% solvent B was used. Purity (%) was determined by reversed-phase HPLC using UV detection (215 nm), and all compounds showed purities greater than 95%. All commercial reagents and solvents were used without further purification. Compound 1 was purchased from ChemDiv.

General Procedure for the Synthesis of N-Phenylphenoxyacetamides 4–26. K₂CO₃ (2.1 equiv, 1.05 mmol, 145 mg) and appropriate phenol (1.05 equiv, 0.53 mmol) were mixed with 2 mL of DMF. The reaction mixture was stirred for 1 h, and then a solution of appropriate 2-chloroacetamide (1 equiv, 0.5 mmol) in 2 mL of DMF was added to the mixture. The reaction was stirred overnight at room temperature and then evaporated under reduced pressure. The residue was dissolved in AcOEt, and the organic phase was washed twice with water, once with a solution of HCl (1 N), and once with brine, then dried over MgSO₄, and evaporated under reduced pressure. The product was purified by flash chromatography or preparative HPLC.

Data for N-(4-benzothiazol-2-ylphenyl)-2-(3-methoxyphenoxy)-acetamide (4): beige powder; yield 61%; purity 98%; ¹H NMR (300 MHz, CDCl₃) δ (ppm) 3.85 (s, 3H), 4.65 (s, 2H), 6.59–6.67 (m, 3H), 7.28 (t, *J* = 8.1 Hz, 1H), 7.40 (dd, *J* = 7.65 Hz, *J* = 7.8 Hz, 1H), 7.51 (dd, *J* = 7.65 Hz, *J* = 8.1 Hz, 1H), 7.78 (d, *J* = 8.7 Hz, 2H), 7.92 (d, *J* = 7.8 Hz, 1H), 8.08 (d, *J* = 8.1 Hz, 1H), 8.11 (d, *J* = 8.7 Hz, 2H), 8.44 (br s, 1H,

NH); ¹³C NMR (75 MHz, CDCl₃) δ 55.43, 67.63, 101.60, 106.80, 108.03, 120.07, 121.62, 123.10, 125.15, 126.37, 128.49, 130.02, 130.47, 134.99, 139.28, 154.16, 158.06, 161.11, 166.34, 167.27; MS [M + H]⁺ *m/z* 391; HRMS (TOF-MS, ES⁺) *m/z* calcd for C₂₂H₁₈N₂O₃S [M + H]⁺ 391.1116, found 391.1115.

Data for N-(4-benzothiazol-2-ylphenyl)-2-(3-cyanophenoxy)-acetamide (5): beige powder; yield 61%; purity 95%; ¹H NMR (300 MHz, CDCl₃) δ (ppm) 4.69 (s, 2H), 7.28–7.32 (m, 2H), 7.39–7.44 (m, 2H), 7.49–7.54 (m, 2H), 7.78 (d, *J* = 8.7 Hz, 2H), 7.93 (d, *J* = 7.5 Hz, 1H), 8.08 (d, *J* = 7.8 Hz, 1H), 8.13 (d, *J* = 8.7 Hz, 2H), 8.34 (br s, 1H, NH); ¹³C NMR (75 MHz, CDCl₃) δ 67.66, 114.03, 118.07, 118.52, 119.50, 120.17, 121.67, 123.17, 125.26, 126.46, 128.63, 130.35, 131.10, 135.07, 139.04, 154.16, 156.93, 165.17, 167.19; MS [M + H]⁺ *m/z* 386; HRMS (TOF-MS, ES⁺) *m/z* calcd for C₂₂H₁₃N₃O₂S [M + H]⁺ 386.0963, found 386.0966.

Data for N-(3,4-dichlorophenyl)-2-(3-phenoxyphenoxy)-acetamide (6): white powder; yield 48%; purity 98%; ¹H NMR (300 MHz, CDCl₃) δ (ppm) 4.60 (s, 2H), 6.65 (t, *J* = 2.4 Hz, 1H), 6.70–6.75 (m, 2H), 7.05–7.08 (m, 2H), 7.18 (t, *J* = 7.5 Hz, 1H), 7.31 (t, *J* = 8.1 Hz, 1H), 7.37–7.44 (m, 4H), 7.85 (d, *J* = 1.8 Hz, 1H), 8.30 (br s, 1H, NH); ¹³C NMR (75 MHz, CDCl₃) δ 67.50, 105.59, 108.90, 112.64, 119.31, 119.51, 121.77, 123.99, 128.21, 129.94, 130.64, 130.74, 132.95, 136.20, 156.68, 157.95, 159.09, 166.07; MS [M – H][–] *m/z* 386.

Data for N-(3,4-dichlorophenyl)-2-(3-methoxyphenoxy)-acetamide (7): white powder; yield 78%; purity 99%; ¹H NMR (300 MHz, CDCl₃) δ (ppm) 3.83 (s, 3H), 4.60 (s, 2H), 6.55–6.66 (m, 3H), 7.23–7.29 (m, 1H), 7.40–7.47 (m, 2H), 7.84 (d, *J* = 2.1 Hz, 1H), 8.28 (br s, 1H, NH); MS [M – H]⁺ *m/z* 326.

Data for N-(3,4-dichlorophenyl)-2-(4-methoxyphenoxy)-acetamide (8): white powder; yield 54%; purity 98%; ¹H NMR (300 MHz, DMSO-*d*₆) δ (ppm) 3.69 (s, 3H), 4.63 (s, 2H), 6.86–6.89 (m, 2H), 6.93–6.96 (m, 2H), 7.56–7.63 (m, 2H), 8.03 (d, *J* = 2.1 Hz, 1H), 10.32 (br s, 1H, NH); MS [M + H]⁺ *m/z* 326.

Data for N-(3,4-dichlorophenyl)-2-[4-(trifluoromethyl)phenoxy]-acetamide (9): white powder; yield 71%; purity >99%; ¹H NMR (300 MHz, CDCl₃) δ (ppm) 4.68 (s, 2H), 7.09 (d, *J* = 8.4 Hz, 2H), 7.42–7.48 (m, 2H), 7.66 (d, *J* = 8.4 Hz, 2H), 7.86 (d, *J* = 1.8 Hz, 1H), 8.24 (br s, 1H, NH); ¹³C NMR (75 MHz, CDCl₃) δ 67.43, 114.88, 119.31, 121.82, 124.02 (q, *J* = 272 Hz), 125.02 (q, *J* = 33 Hz), 127.50, 128.43, 130.69, 133.03, 136.06, 159.02, 165.45; MS [M – H][–] *m/z* 362.

Data for 2-(4-chlorophenoxy)-N-(3,4-dichlorophenyl)acetamide (10): beige powder; yield 68%; purity 98%; ¹H NMR (300 MHz, CDCl₃) δ (ppm) 4.60 (s, 2H), 6.93–6.96 (m, 2H), 7.32–7.35 (m, 2H), 7.43–7.47 (m, 2H), 7.85 (d, *J* = 1.5 Hz, 1H), 8.25 (br s, 1H, NH); MS [M – H][–] *m/z* 328.

Data for N-(3,4-dichlorophenyl)-2-p-tolylxyacetamide (11): white powder; yield 33%; purity >99%; ¹H NMR (300 MHz, DMSO-*d*₆) δ (ppm) 2.23 (s, 3H), 4.66 (s, 2H), 6.89 (d, *J* = 8.1 Hz, 2H), 7.10 (d, *J* = 8.1 Hz, 2H), 7.55–7.62 (m, 2H), 8.02 (d, *J* = 1.5 Hz, 1H), 10.33 (br s, 1H, NH); MS [M – H][–] *m/z* 308.

Data for N-1,3-benzodioxol-5-yl-2-(biphenyl-4-yloxy)acetamide (12): beige powder; yield 49%; purity 95%; ¹H NMR (300 MHz, CDCl₃) δ (ppm) 4.66 (s, 2H), 5.99 (s, 2H), 6.80 (d, *J* = 8.4 Hz, 1H), 6.91 (dd, *J* = 2.1 Hz, *J* = 8.4 Hz, 1H), 7.05–7.10 (m, 2H), 7.33 (d, *J* = 2.1 Hz, 1H), 7.35–7.38 (m, 1H), 7.43–7.48 (m, 2H), 7.57–7.62 (m, 4H), 8.22 (br s, 1H, NH); ¹³C NMR (75 MHz, CDCl₃) δ 67.68, 101.41, 103.02, 108.16, 113.53, 115.14, 126.83, 127.11, 128.57, 128.85, 131.02, 135.58, 140.28, 144.78, 147.93, 156.51, 166.05; MS [M + H]⁺ *m/z* 348.

Data for N-1,3-benzodioxol-5-yl-2-[4-(trifluoromethyl)phenoxy]-acetamide (13): beige powder; yield 66%; purity 99%; ¹H NMR (300 MHz, DMSO-*d*₆) δ (ppm) 4.77 (s, 2H), 5.98 (s, 2H), 6.86 (d, *J* = 8.4 Hz, 1H), 7.01 (dd, *J* = 2.1 Hz, *J* = 8.4 Hz, 1H), 7.14–7.18 (m, 2H), 7.30 (d, *J* = 2.1 Hz, 1H), 7.66–7.70 (m, 2H), 10.04 (br s, 1H, NH); ¹³C NMR (75 MHz, DMSO-*d*₆) δ 67.48, 101.51, 102.32, 108.50, 113.13, 115.68, 122.14 (q, *J* = 33 Hz), 124.98 (q, *J* = 272 Hz), 127.45, 133.06, 143.75, 147.52, 161.15, 166.08; MS [M + H]⁺ *m/z* 340.

Data for N-1,3-benzodioxol-5-yl-2-(3-phenoxyphenoxy)-acetamide (14): beige powder; yield 61%; purity 95%; ¹H NMR (300 MHz, DMSO-*d*₆) δ (ppm) 4.64 (s, 2H), 5.98 (s, 2H), 6.59 (dd, *J* = 1.8 Hz, *J* = 8.1 Hz, 1H), 6.65 (t, *J* = 2.1 Hz, 1H), 6.76 (dd, *J* = 2.1 Hz,

$J = 8.1$ Hz, 1H), 6.86 (d, $J = 8.4$ Hz, 1H), 7.00–7.04 (m, 3H), 7.12–7.17 (m, 1H), 7.27–7.40 (m, 4H), 9.94 (br s, 1H, NH); MS $[M + H]^+ m/z$ 364.

Data for 2-(2-fluorophenoxy)-N-(2-methylquinolin-6-yl)-acetamide (15): white powder; yield 13%; purity >99%; ^1H NMR (300 MHz, CDCl_3) δ (ppm) 2.78 (s, 3H), 4.74 (s, 2H), 7.03–7.23 (m, 4H), 7.33 (d, $J = 8.4$ Hz, 1H), 7.68 (dd, $J = 2.4$ Hz, $J = 9.0$ Hz, 1H), 8.09 (d, $J = 9.0$ Hz, 1H), 8.11 (d, $J = 8.4$ Hz, 1H), 8.42 (d, $J = 2.4$ Hz, 1H), 8.72 (br s, 1H, NH); ^{13}C NMR (75 MHz, CDCl_3) δ 24.52, 69.19, 116.30, 116.46, 116.79 (d, $J = 18$ Hz), 122.93, 123.45 (d, $J = 7$ Hz), 123.52, 124.87 (d, $J = 4$ Hz), 127.00, 128.65, 134.30, 136.90, 144.45, 145.35 (d, $J = 10$ Hz), 152.80 (d, $J = 245$ Hz), 158.24, 166.17; MS $[M + H]^+ m/z$ 311; HRMS (TOF-MS, ES^+) m/z calcd for $\text{C}_{18}\text{H}_{15}\text{FN}_2\text{O}_2$ $[M + H]^+$ 311.1196, found 311.1191.

Data for 2-(3-methoxyphenoxy)-N-(2-methylquinolin-6-yl)-acetamide (16): white powder; yield 13%; purity >99%; ^1H NMR (300 MHz, CDCl_3) δ (ppm) 2.75 (s, 3H), 3.84 (s, 3H), 4.68 (s, 2H), 6.59–6.67 (m, 3H), 7.25–7.31 (m, 1H), 7.31 (d, $J = 8.4$ Hz, 1H), 7.65 (dd, $J = 2.4$ Hz, $J = 9.0$ Hz, 1H), 8.02 (d, $J = 9.0$ Hz, 1H), 8.06 (d, $J = 8.4$ Hz, 1H), 8.37 (d, $J = 2.4$ Hz, 1H), 8.48 (br s, 1H, NH); ^{13}C NMR (75 MHz, CDCl_3) δ 25.23, 55.41, 67.71, 101.61, 106.81, 108.01, 116.64, 122.73, 123.16, 126.87, 129.50, 130.51, 134.00, 136.14, 145.42, 158.12, 158.41, 161.11, 166.44; MS $[M + H]^+ m/z$ 323.

Data for 2-(3,4-difluorophenoxy)-N-(4-phenoxyphenyl)-acetamide (17): beige powder; yield 87%; purity 96%; ^1H NMR (300 MHz, CDCl_3) δ (ppm) 4.59 (s, 2H), 6.71–6.76 (m, 1H), 6.84–6.91 (m, 1H), 7.00–7.05 (m, 4H), 7.10–7.21 (m, 2H), 7.35–7.38 (m, 2H), 7.54–7.58 (m, 2H), 8.16 (br s, 1H, NH); ^{13}C NMR (75 MHz, CDCl_3) δ 68.22, 105.07 (d, $J = 20$ Hz), 110.05, 117.78 (d, $J = 20$ Hz), 118.63, 119.59, 122.00, 123.31, 129.80, 131.99, 146.16 (dd, $J = 13$ Hz, $J = 243$ Hz), 150.72 (dd, $J = 14$ Hz, $J = 249$ Hz), 153.12 (d, $J = 8$ Hz), 154.23, 157.31, 165.39; MS $[M + H]^+ m/z$ 356.

Data for 2-(3-methoxyphenoxy)-N-(4-phenoxyphenyl)acetamide (18): white powder; yield 71%; purity >99%; ^1H NMR (300 MHz, $\text{DMSO}-d_6$) δ (ppm) 3.73 (s, 3H), 4.66 (s, 2H), 6.55–6.59 (m, 3H), 6.95–7.02 (m, 4H), 7.07–7.12 (m, 1H), 7.18–7.23 (m, 1H), 7.34–7.39 (m, 2H), 7.64–7.67 (m, 2H), 10.09 (br s, 1H, NH); MS $[M + H]^+ m/z$ 350.

Data for 2-(3,4-dichlorophenoxy)-N-[4-(trifluoromethyl)phenyl]-acetamide (19): white powder; yield 76%; purity >99%; ^1H NMR (300 MHz, $\text{DMSO}-d_6$) δ (ppm) 4.82 (s, 2H), 7.01–7.09 (m, 1H), 7.30–7.36 (m, 1H), 7.52–7.60 (m, 1H), 7.66–7.73 (m, 2H), 7.82–7.88 (m, 2H), 10.46 (br s, 1H, NH); ^{13}C NMR (75 MHz, $\text{DMSO}-d_6$) δ 67.77, 116.05, 117.35, 120.00, 123.57, 124.21 (q, $J = 32$ Hz), 124.78 (q, $J = 272$ Hz), 126.59, 131.45, 131.99, 142.35, 157.72, 167.11; MS $[M - H]^- m/z$ 362.

Data for 2-(3,4-difluorophenoxy)-N-[4-(trifluoromethyl)phenyl]-acetamide (20): white powder; yield 70%; purity >99%; ^1H NMR (300 MHz, $\text{DMSO}-d_6$) δ (ppm) 4.77 (s, 2H), 6.83–6.87 (m, 1H), 7.12–7.19 (m, 1H), 7.33–7.43 (m, 1H), 7.69 (d, $J = 8.4$ Hz, 2H), 7.85 (d, $J = 8.4$ Hz, 2H), 10.43 (br s, 1H, NH); MS $[M - H]^- m/z$ 330.

Data for N-(4-chlorophenyl)-2-(3-methoxyphenoxy)acetamide (21): white powder; yield 60%; purity >99%; ^1H NMR (300 MHz, $\text{DMSO}-d_6$) δ (ppm) 3.73 (s, 3H), 4.67 (s, 2H), 6.55–6.58 (m, 3H), 7.17–7.23 (m, 1H), 7.36–7.39 (m, 2H), 7.66–7.69 (m, 2H), 10.20 (br s, 1H, NH); ^{13}C NMR (75 MHz, CDCl_3) δ 55.60, 67.67, 101.62, 107.22, 107.39, 121.75, 127.78, 129.11, 130.50, 137.80, 159.43, 160.92, 167.17; MS $[M + H]^+ m/z$ 292.

Data for N-biphenyl-4-yl-2-(3-methoxyphenoxy)acetamide (22): white powder; yield 52%; purity >99%; ^1H NMR (300 MHz, $\text{DMSO}-d_6$) δ (ppm) 3.74 (s, 3H), 4.70 (s, 2H), 6.56–6.60 (m, 3H), 7.18–7.24 (m, 1H), 7.29–7.35 (m, 1H), 7.42–7.47 (m, 2H), 7.63–7.66 (m, 4H), 7.73–7.76 (m, 2H), 10.17 (br s, 1H, NH); MS $[M + H]^+ m/z$ 334.

Data for 2-(3-phenoxyphenoxy)-N-phenylacetamide (23): white powder; yield 45%; purity 98%; ^1H NMR (300 MHz, CDCl_3) δ (ppm) 4.60 (s, 2H), 6.67–6.69 (m, 1H), 6.71–6.75 (m, 2H), 7.07 (d, $J = 7.8$ Hz, 2H), 7.16–7.20 (m, 2H), 7.31 (t, $J = 8.1$ Hz, 1H), 7.35–7.42 (m, 4H), 7.60 (d, $J = 7.8$ Hz, 2H), 8.24 (br s, 1H, NH); MS $[M + H]^+ m/z$ 320.

Data for N-(4-cyanophenyl)-2-(3-phenoxyphenoxy)acetamide (24): white powder; yield 64%; purity >99%; ^1H NMR (300 MHz, $\text{DMSO}-d_6$) δ (ppm) 4.74 (s, 2H), 6.59 (dd, $J = 1.8$ Hz, $J = 8.1$ Hz, 1H), 6.64 (t, $J = 2.1$ Hz, 1H), 6.77 (dd, $J = 1.8$ Hz, $J = 8.1$ Hz, 1H), 7.00–7.03

(m, 2H), 7.11–7.16 (m, 1H), 7.30 (t, $J = 8.1$ Hz, 1H), 7.35–7.40 (m, 2H), 7.77–7.82 (m, 4H), 10.49 (br s, 1H, NH); ^{13}C NMR (75 MHz, $\text{DMSO}-d_6$) δ 67.59, 105.80, 105.94, 110.00, 111.67, 119.36, 120.13, 124.17, 130.51, 131.07, 133.74, 143.04, 156.67, 158.35, 159.51, 167.67; MS $[M - H]^- m/z$ 343.

Data for N-(3-cyanophenyl)-2-(3-phenoxyphenoxy)acetamide (25): white powder; yield 53%; purity >99%; ^1H NMR (300 MHz, $\text{DMSO}-d_6$) δ (ppm) 4.72 (s, 2H), 6.60 (dd, $J = 1.8$ Hz, $J = 8.1$ Hz, 1H), 6.65 (t, $J = 2.1$ Hz, 1H), 6.78 (dd, $J = 1.8$ Hz, $J = 8.1$ Hz, 1H), 6.97–7.03 (m, 2H), 7.11–7.16 (m, 1H), 7.31 (t, $J = 8.1$ Hz, 1H), 7.35–7.41 (m, 2H), 7.49–7.57 (m, 2H), 7.85–7.91 (m, 1H), 8.09–8.11 (m, 1H), 10.39 (br s, 1H, NH); MS $[M - H]^- m/z$ 343.

Data for N-(3-methoxyphenoxy)-2-[4-(trifluoromethyl)phenoxy]-acetamide (26): white powder; yield 46%; purity 95%; ^1H NMR (300 MHz, $\text{DMSO}-d_6$) δ (ppm) 3.72 (s, 3H), 4.81 (s, 2H), 6.64–6.68 (m, 1H), 7.15–7.35 (m, 4H), 7.31 (t, $J = 2.1$ Hz, 1H), 7.66–7.71 (m, 2H), 10.13 (br s, 1H, NH); MS $[M - H]^- m/z$ 324.

N-(4-Benzothiazol-2-ylphenyl)-2-[3-(methoxyphenyl)sulfanyl]-acetamide (27): K_2CO_3 (1.05 equiv, 0.53 mmol, 73 mg) and 3-methoxythiophenol (1.05 equiv, 0.53 mmol) were mixed with 2 mL of DMF. The reaction mixture was stirred for 1 h, and then a solution of N-(4-benzothiazol-2-ylphenyl)-2-chloroacetamide (2[22]; 1 equiv, 0.5 mmol, 151 mg) in 2 mL of DMF was added to the mixture. The reaction was stirred overnight at room temperature and then evaporated under reduced pressure. The residue was dissolved in AcOEt, and the organic phase was washed twice with water, once with a solution of HCl (1 N), and once with brine, then dried over MgSO_4 , and evaporated under reduced pressure. The product was purified by flash chromatography (cyclohexane/AcOEt = 95/5 to 9/1): beige powder; yield 72%; purity 95%; ^1H NMR (300 MHz, CDCl_3) δ (ppm) 3.80 (s, 3H), 3.82 (s, 2H), 6.80 (dd, $J = 2.4$ Hz, $J = 8.1$ Hz, 1H), 6.92–6.97 (m, 2H), 7.27 (t, $J = 8.1$ Hz, 1H), 7.39 (dd, $J = 7.8$ Hz, $J = 8.1$ Hz, 1H), 7.51 (dd, $J = 7.8$ Hz, $J = 8.1$ Hz, 1H), 7.66 (d, $J = 8.7$ Hz, 2H), 7.91 (d, $J = 7.8$ Hz, 1H), 8.07 (d, $J = 7.8$ Hz, 1H), 8.07 (d, $J = 8.7$ Hz, 2H), 8.72 (br s, 1H, NH); ^{13}C NMR (75 MHz, CDCl_3) δ 38.46, 55.34, 112.89, 114.04, 119.85, 120.46, 121.62, 123.05, 125.15, 126.38, 128.42, 129.82, 130.46, 134.94, 135.17, 139.75, 154.08, 160.02, 166.35, 167.31; MS $[M + H]^+ m/z$ 407.

■ ASSOCIATED CONTENT

Supporting Information

General procedure for the synthesis of 2-chloroacetamide and 2-chloropropionamide, characterization of starting materials 2[1–38], general procedure for the synthesis of the library and purity of 118 compounds randomly selected from the library, and effect of compound 4 on the susceptibility of *M. tuberculosis* H37Rv measured by Bactec MGIT960. This material is available free of charge via the Internet at <http://pubs.acs.org>.

Accession Codes

PDB ID codes 3Q3S and 4DW6.

■ AUTHOR INFORMATION

Corresponding Author

*E-mail: benoit.deprez@univ-lille2.fr. Phone: +33 320 964 947. Fax: +33 320 964 709. URL: <http://www.deprezlab.fr> (U761); <http://www.drugdiscoverylille.org> (PRIM).

Present Address

*Galapagos N.V., General De Wittelaan L11 A3, 2800 Mechelen, Belgium.

Author Contributions

▣ These authors contributed equally to this work.

Notes

The authors declare no competing financial interest.

ACKNOWLEDGMENTS

We thank Vincent Van Geem, Dr. Bertrand Dirie, Stéphanie Devassine, and Aurore Muller for technical assistance, Nicolas Blondiaux for the Bactec experiments, Dr. Sameh H. Soror for data collection, and Prof. André Tartar for scientific discussion. We are grateful to the institutions that support our laboratory (INSERM, INSERM-Avenir fellowship to P.B., Institut Pasteur Korea (Grants K204EA000001-08E0100-00100 and K204EA000001-09E0100-00100), Université de Lille Nord de France, Institut Pasteur de Lille, CNRS, European Union, Région Nord-Pas de Calais, Fonds européen de développement régional (FEDER) (Grants 09220019 and 09220020 PRESAGE 31510), Agence Nationale de la Recherche (ANR; Grant ANR-06-EMPB-033), PRIM (Projet Phare CPER TB DRUG BOOST Grant 11002859). R.W. is a Research Associate at the Belgian Fund for Scientific Research (FNRS). We are grateful to the SLS-PX3 beamline scientists for support during data acquisition and the European Synchrotron Radiation Facility (ESRF; Group BAG MX-485). Data management was performed using Pipeline Pilot from Accelrys. We thank Varian Inc. for their technical support. RMN acquisitions were done at the Laboratoire d'Application de Résonance Magnétique Nucléaire (LARMN), Lille, France.

ABBREVIATIONS USED

AcOEt, ethyl acetate; Boc, *tert*-butoxycarbonyl; DIEA, diisopropylethylamine; DMA, dimethylacetamide; DMF, dimethylformamide; DMSO, dimethyl sulfoxide; DRC, dose–response curve; GFP, green fluorescent protein; HTH, helix–turn–helix; MDR, multi-drug-resistant; MeOH, methanol; MIC, minimal inhibitory concentration; MU, 4-methylumbelliferone; MUG, 4-methylumbelliferyl β -D-glucuronide; PBS, phosphate-buffered saline; Ph, phenyl; rt, room temperature; SAR, structure–activity relationship; TB, tuberculosis; TFA, trifluoroacetic acid; TSA, thermal shift assay

REFERENCES

- (1) World Health Organization. *Global Tuberculosis Control*; World Health Organization: Geneva, Switzerland, 2011; ISBN 978-92-4-156438-0.
- (2) Cox, H. S.; Ford, N.; Reeder, J. C. Are we really that good at treating tuberculosis? *Lancet Infect. Dis.* **2009**, *9*, 138–139.
- (3) Kaufmann, S. H. E.; McMichael, A. J. Annulling a dangerous liaison: vaccination strategies against AIDS and tuberculosis. *Nat. Med.* **2005**, *11*, S33–S44.
- (4) Elzinga, G.; Raviglione, M. C.; Maher, D. Scale up: meeting targets in global tuberculosis control. *Lancet* **2004**, *363*, 814–819.
- (5) Dye, C.; Maher, D.; Weil, D.; Espinal, M.; Raviglione, M. Targets for global tuberculosis control [short communication]. *Int. J. Tuberc. Lung Dis.* **2006**, *10*, 460–462.
- (6) Chaisson, R. E.; Martinson, N. A. Tuberculosis in Africa—combating an HIV-driven crisis. *N. Engl. J. Med.* **2008**, *358*, 1089–1092.
- (7) Villemagne, B.; Crauste, C.; Flipo, M.; Baulard, A. R.; Déprez, B.; Willand, N. Tuberculosis: the drug development pipeline at a glance. *Eur. J. Med. Chem.* **2012**, *51*, 1–16.
- (8) Baulard, A. R.; Betts, J. C.; Engohang-Ndong, J.; Quan, S.; McAdam, R. A.; Brennan, P. J.; Loch, C.; Besra, G. S. Activation of the pro-drug ethionamide is regulated in mycobacteria. *J. Biol. Chem.* **2000**, *275*, 28326–28331.
- (9) Fraaije, M. W.; Kamerbeek, N. M.; Heidekamp, A. J.; Fortin, R.; Janssen, D. B. The prodrug activator EtaA from *Mycobacterium tuberculosis* is a Baeyer-Villiger monooxygenase. *J. Biol. Chem.* **2004**, *279*, 3354–3360.
- (10) Hanouille, X.; Wieruszkeski, J.-M.; Rousselot-Pailley, P.; Landrieu, I.; Loch, C.; Lippens, G.; Baulard, A. R. Selective intracellular accumulation of the major metabolite issued from the activation of the prodrug ethionamide in mycobacteria. *J. Antimicrob. Chemother.* **2006**, *58*, 768–772.
- (11) Hanouille, X.; Wieruszkeski, J.-M.; Rousselot-Pailley, P.; Landrieu, I.; Baulard, A. R.; Lippens, G. Monitoring of the ethionamide pro-drug activation in mycobacteria by (1)H high resolution magic angle spinning NMR. *Biochem. Biophys. Res. Commun.* **2005**, *331*, 452–458.
- (12) DeBarber, A. E.; Mdluli, K.; Bosman, M.; Bekker, L.-G.; Barry, C. E. Ethionamide activation and sensitivity in multidrug-resistant *Mycobacterium tuberculosis*. *Proc. Natl. Acad. Sci. U.S.A.* **2000**, *97*, 9677–9682.
- (13) Kremer, L.; Dover, L. G.; Morbidoni, H. R.; Vilcheze, C.; Maughan, W. N.; Baulard, A.; Tu, S.-C.; Honore, N.; Deretic, V.; Sacchettini, J. C.; Loch, C.; Jacobs, W. R., Jr.; Besra, G. S. Inhibition of InhA activity, but not KasA activity, induces formation of a KasA-containing complex in mycobacteria. *J. Biol. Chem.* **2003**, *278*, 20547–20554.
- (14) Wang, F.; Langley, R.; Gulten, G.; Dover, L. G.; Besra, G. S.; Jacobs, W. R., Jr.; Sacchettini, J. C. Mechanism of thioamide drug action against tuberculosis and leprosy. *J. Exp. Med.* **2007**, *204*, 73–78.
- (15) Engohang-Ndong, J.; Baillat, D.; Aumercier, M.; Bellefontaine, F.; Besra, G. S.; Loch, C.; Baulard, A. R. EthR, a repressor of the TetR/CamR family implicated in ethionamide resistance in mycobacteria, octamerizes cooperatively on its operator. *Mol. Microbiol.* **2004**, *51*, 175–188.
- (16) Willand, N.; Dirie, B.; Carette, X.; Bifani, P.; Singhal, A.; Desroses, M.; Leroux, F.; Willery, E.; Mathys, V.; Deprez-Poulain, R.; Delcroix, G.; Frenois, F.; Aumercier, M.; Loch, C.; Villeret, V.; Deprez, B.; Baulard, A. R. Synthetic EthR inhibitors boost antituberculous activity of ethionamide. *Nat. Med.* **2009**, *15*, 537–544.
- (17) Flipo, M.; Desroses, M.; Lecat-Guillet, N.; Dirie, B.; Carette, X.; Leroux, F.; Piveteau, C.; Demirkaya, F.; Lens, Z.; Rucktooa, P.; Villeret, V.; Christophe, T.; Jeon, H. K.; Loch, C.; Brodin, P.; Déprez, B.; Baulard, A. R.; Willand, N. Ethionamide boosters: synthesis, biological activity, and structure–activity relationships of a series of 1,2,4-oxadiazole EthR inhibitors. *J. Med. Chem.* **2011**, *54*, 2994–3010.
- (18) Flipo, M.; Desroses, M.; Lecat-Guillet, N.; Villemagne, B.; Blondiaux, N.; Leroux, F.; Piveteau, C.; Mathys, V.; Flament, M.-P.; Siepmann, J.; Villeret, V.; Wohlkönig, A.; Wintjens, R.; Soror, S. H.; Christophe, T.; Jeon, H. K.; Loch, C.; Brodin, P.; Deprez, B.; Baulard, A. R.; Willand, N. Ethionamide boosters. 2. Combining bioisosteric replacement and structure-based drug design to solve pharmacokinetic issues in a series of potent 1,2,4-oxadiazole EthR inhibitors. *J. Med. Chem.* **2012**, *55*, 68–83.
- (19) Willand, N.; Desroses, M.; Toto, P.; Dirie, B.; Lens, Z.; Villeret, V.; Rucktooa, P.; Loch, C.; Baulard, A.; Deprez, B. Exploring drug target flexibility using in situ click chemistry: application to a mycobacterial transcriptional regulator. *ACS Chem. Biol.* **2010**, *5*, 1007–1013.
- (20) Carette, X.; Blondiaux, N.; Willery, E.; Hoos, S.; Lecat-Guillet, N.; Lens, Z.; Wohlkönig, A.; Wintjens, R.; Soror, S. H.; Frénois, F.; Dirie, B.; Villeret, V.; England, P.; Lippens, G.; Deprez, B.; Loch, C.; Willand, N.; Baulard, A. R. Structural activation of the transcriptional repressor EthR from *Mycobacterium tuberculosis* by single amino acid change mimicking natural and synthetic ligands. *Nucleic Acids Res.* **2012**, *40*, 3018–3030.
- (21) Lo, M.-C.; Aulabaugh, A.; Jin, G.; Cowling, R.; Bard, J.; Malamas, M.; Ellestad, G. Evaluation of fluorescence-based thermal shift assays for hit identification in drug discovery. *Anal. Biochem.* **2004**, *332*, 153–159.
- (22) Niesen, F. H.; Berglund, H.; Vedadi, M. The use of differential scanning fluorimetry to detect ligand interactions that promote protein stability. *Nat. Protoc.* **2007**, *2*, 2212–2221.
- (23) Matulis, D.; Kranz, J. K.; Salemme, F. R.; Todd, M. J. Thermodynamic stability of carbonic anhydrase: measurements of binding affinity and stoichiometry using ThermoFluor. *Biochemistry* **2005**, *44*, 5258–5266.
- (24) Senisterra, G. A.; Markin, E.; Yamazaki, K.; Hui, R.; Vedadi, M.; Awrey, D. E. Screening for ligands using a generic and high-throughput light-scattering-based assay. *J. Biomol. Screening* **2006**, *11*, 940–948.
- (25) Vedadi, M.; Niesen, F. H.; Allali-Hassani, A.; Fedorov, O. Y.; Finerty, P. J.; Wasney, G. A.; Yeung, R.; Arrowsmith, C.; Ball, L. J.; Berglund, H.; Hui, R.; Marsden, B. D.; Nordlund, P.; Sundstrom, M.;

Weigelt, J.; Edwards, A. M. Chemical screening methods to identify ligands that promote protein stability, protein crystallization, and structure determination. *Proc. Natl. Acad. Sci. U.S.A.* **2006**, *103*, 15835–15840.

(26) Frénois, F.; Engohang-Ndong, J.; Lochter, C.; Baulard, A. R.; Villeret, V. Structure of EthR in a ligand bound conformation reveals therapeutic perspectives against tuberculosis. *Mol. Cell* **2004**, *16*, 301–307.

(27) Lipinski, C. A.; Lombardo, F.; Dominy, B. W.; Feeney, P. J. Experimental and computational approaches to estimate solubility and permeability in drug discovery and development settings. *Adv. Drug Delivery Rev.* **2001**, *46*, 3–26.

(28) Lipinski, C. A. Lead- and drug-like compounds: the rule-of-five revolution. *Drug Discovery Today: Technol.* **2004**, *1*, 337–341.

(29) Veber, D. F.; Johnson, S. R.; Cheng, H.-Y.; Smith, B. R.; Ward, K. W.; Kopple, K. D. Molecular properties that influence the oral bioavailability of drug candidates. *J. Med. Chem.* **2002**, *45*, 2615–2623.

(30) Cvetovich, R. J.; DiMichele, L. Formation of acrylamides, acrylamides, and amides directly from carboxylic acids using thionyl chloride in dimethylacetamide in the absence of bases. *Org. Process Res. Dev.* **2006**, *10*, 944–946.

(31) Christophe, T.; Ewann, F.; Jeon, H. K.; Cechetto, J.; Brodin, P. High-content imaging of *Mycobacterium tuberculosis*-infected macrophages: an in vitro model for tuberculosis drug discovery. *Future Med. Chem.* **2010**, *2*, 1283–1293.

(32) Christophe, T.; Jackson, M.; Jeon, H. K.; Fenistein, D.; Contreras-Dominguez, M.; Kim, J.; Genovesio, A.; Carralot, J.-P.; Ewann, F.; Kim, E. H.; Lee, S. Y.; Kang, S.; Seo, M. J.; Park, E. J.; Skovierova, H., H.; Pham, H.; Riccardi, G.; Nam, J. Y.; Marsollier, L.; Kempf, M.; Joly-Guillou, M.-L.; Oh, T.; Shin, W. K.; No, Z.; Nehrbass, U.; Brosch, R.; Cole, S. T.; Brodin, P. High content screening identifies decaprenyl-phosphoribose 2' epimerase as a target for intracellular antimycobacterial inhibitors. *PLoS Pathog.* **2009**, *5*, e1000645.

(33) Brodin, P.; Christophe, T. High-content screening in infectious diseases. *Curr. Opin. Chem. Biol.* **2011**, *15*, 534–539.

(34) Ehrmann, M.; Bolek, P.; Mondigler, M.; Boyd, D.; Lange, R. TnTIN and TnTAP: mini-transposons for site-specific proteolysis *in vivo*. *Proc. Natl. Acad. Sci. U.S.A.* **1997**, *94*, 13111–13115.

(35) Picardeau, M.; Le Dantec, C.; Vincent, V. Analysis of the internal replication region of a mycobacterial linear plasmid. *Microbiology* **2000**, *146*, 305–313.

(36) Snapper, S. B.; Melton, R. E.; Mustafa, S.; Kieser, T.; Jacobs, W. R., Jr. Isolation and characterization of efficient plasmid transformation mutants of *Mycobacterium smegmatis*. *Mol. Microbiol.* **1990**, *4*, 1911–1919.

(37) Murshudov, G. N.; Vagin, A. A.; Dodson, E. J. Refinement of macromolecular structures by the maximum-likelihood method. *Acta Crystallogr., Sect. D: Biol. Crystallogr.* **1997**, *53*, 240–255.

(38) Emsley, P.; Cowtan, K. Coot: model-building tools for molecular graphics. *Acta Crystallogr., Sect. D: Biol. Crystallogr.* **2004**, *60*, 2126–2132.

(39) Wallace, A. C.; Laskowski, R. A.; Thornton, J. M. LIGPLOT: a program to generate schematic diagrams of protein-ligand interactions. *Protein Eng.* **1995**, *8*, 127–134.